

# Influence of B substituting for Al on the structure and magnetic properties of the bulk $\text{Nd}_{60}\text{Fe}_{20}\text{Al}_{10-x}\text{Co}_{10}\text{B}_x$ amorphous alloys

H. XU, X. H. TAN, Q. BAI, Q. WANG, Y. D. DONG

*Institute of Materials Science, Shanghai University, Shanghai 200072, People's Republic of China*

*E-mail: hxu@mail.shu.edu.cn*

**Published online:** 16 September 2005

Bulk amorphous alloys from the Nd(Pr)-Fe(Co)-Al system have attracted considerable interest because of their potential for use as permanent magnets with high coercivity. In particular, the  $\text{Nd}_{60}\text{Fe}_{20}\text{Al}_{10}\text{Co}_{10}$  exhibits some remarkable features such as the absence of a glass endothermic reaction to glass transition temperature, hard-magnetic behavior, and the good glass forming ability claimed attractive [1–5]. It is proposed that the high coercivity is due to the formation of ordered clusters with large random magnetic anisotropy in the amorphous matrix. Elemental substitution is considered to be an effective way to improve magnetic properties. It has been demonstrated that B alloying additions can enhance coercivity for Nd-Fe-Al system while maintaining the high glass forming ability [6, 7]. Furthermore,  $\text{Nd}_2\text{Fe}_{14}\text{B}$  phase might be precipitated and improve magnetic properties. The aim of this paper is to study the influence of B substitution for Al on the structure and magnetic properties of  $\text{Nd}_{60}\text{Fe}_{20}\text{Al}_{10-x}\text{Co}_{10}\text{B}_x$  alloys ( $x = 0, 2, 5$ ).

Alloy ingots of nominal composition of  $\text{Nd}_{60}\text{Fe}_{20}\text{Al}_{10-x}\text{Co}_{10}\text{B}_x$  ( $x = 0, 2, 5$ ) were prepared by arc melting mixtures of the pure elements Nd, Fe, Al and Co and Fe-B alloy in an argon atmosphere. The sheet specimens (dimensions 1 mm × 10 mm × 50 mm) were obtained by suction casting of the molten alloy into a copper mold. The crystallization processes of the amorphous alloys were investigated by using a Perkin-Elmer differential scanning calorimeter (DSC). The structural analysis was carried out using X-ray diffractometry (XRD) with a Siemens D5000 diffractometer using  $\text{Cu-K}\alpha$  radiation and a HITACHI S-570 scanning electron microscope (SEM) equipped with energy dispersive spectroscopy (EDS). Magnetic measurements were performed using a vibrating sample magnetometer (VSM) with a maximum applied field of 1.8 T.

Fig. 1 shows the X-ray diffraction patterns of as-cast  $\text{Nd}_{60}\text{Fe}_{20}\text{Al}_{10-x}\text{Co}_{10}\text{B}_x$  ( $x = 0, 2, 5$ ) samples. No obvious crystalline peaks were found for the  $\text{Nd}_{60}\text{Fe}_{20}\text{Co}_{10}\text{Al}_{10}$  (i.e.,  $x = 0$ ) alloy. Upon addition of 2 at.% B, the as-cast sample has a small amount of hexagonal Nd phase coexisting with an amorphous matrix. On increasing the B content to 5 at.%, more crystalline diffraction peaks, which can be identified as hexagonal Nd phase,  $\text{NdFe}_4\text{B}_4$  phase and an unknown phase (U phase), are observed. This suggests that the

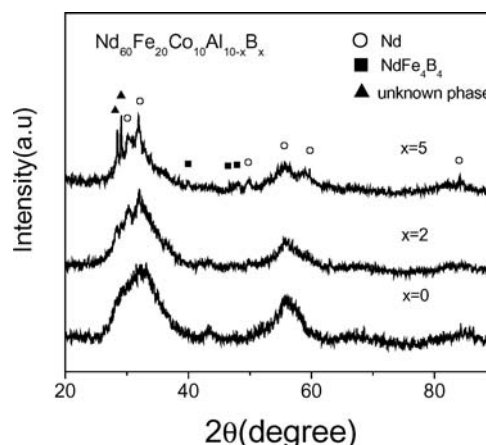


Figure 1 XRD patterns of as-cast  $\text{Nd}_{60}\text{Fe}_{20}\text{Co}_{10}\text{Al}_{10-x}\text{B}_x$  ( $x = 0, 2, 5$ ) alloys.

glass forming ability of  $\text{Nd}_{60}\text{Fe}_{20}\text{Al}_{10-x}\text{Co}_{10}\text{B}_x$  ( $x = 0, 2, 5$ ) alloys decreases with increasing additions of B.

Fig. 2 shows SEM images of the as-cast  $\text{Nd}_{60}\text{Fe}_{20}\text{Al}_{10-x}\text{Co}_{10}\text{B}_x$  ( $x = 0, 2, 5$ ) alloys. The lack of obvious contrast in Fig. 2a, indicates that an amorphous structure is formed in the as-cast  $\text{Nd}_{60}\text{Fe}_{20}\text{Al}_{10}\text{Co}_{10}$  alloy. Both Fig. 2b and c display a matrix (A) and a dark irregularly shaped second phase (B). Moreover, some gray regions (marked C) are observed in Fig. 2c. The local average elemental compositions (except for boron) were obtained using EDX analysis. The results are shown in Table I. It is revealed that the region B is Nd-rich phase ( $\approx \text{Nd}_{74}\text{Fe}_{10}\text{Al}_7\text{Co}_9$  and  $\text{Nd}_{73}\text{Fe}_{13}\text{Al}_5\text{Co}_9$  for  $x = 2$  and  $x = 5$  alloys, respectively). The region C is Fe-rich phase ( $\approx \text{Nd}_{44}\text{Fe}_{44}\text{Al}_3\text{Co}_9$ ).

The DSC curves obtained at a constant heating rate of 20 K/min for the as-cast  $\text{Nd}_{60}\text{Fe}_{20}\text{Al}_{10-x}\text{Co}_{10}\text{B}_x$  ( $x$

TABLE I EDS analysis of as-cast samples of  $\text{Nd}_{60}\text{Fe}_{20}\text{Al}_{10-x}\text{Co}_{10}\text{B}_x$  ( $x = 0, 2, 5$ ).

| Alloy (at.%) | $\text{Nd}_{60}\text{Fe}_{20}\text{Al}_{10}\text{Co}_{10}$ | $\text{Nd}_{60}\text{Fe}_{20}\text{Al}_8\text{Co}_{10}\text{B}_2$ |    | $\text{Nd}_{60}\text{Fe}_{20}\text{Al}_5\text{Co}_{10}\text{B}_5$ |    |    |
|--------------|--|---|----|---|----|----|
|              | Matrix A   | Matrix A  | B  | Matrix A  | B  | C  |
| Nd           | 61   | 60  | 74 | 61  | 73 | 44 |
| Fe           | 20   | 19  | 10 | 20  | 13 | 44 |
| Al           | 9  | 10  | 7  | 7   | 5  | 3  |
| Co           | 10   | 11  | 9  | 12  | 9  | 9  |

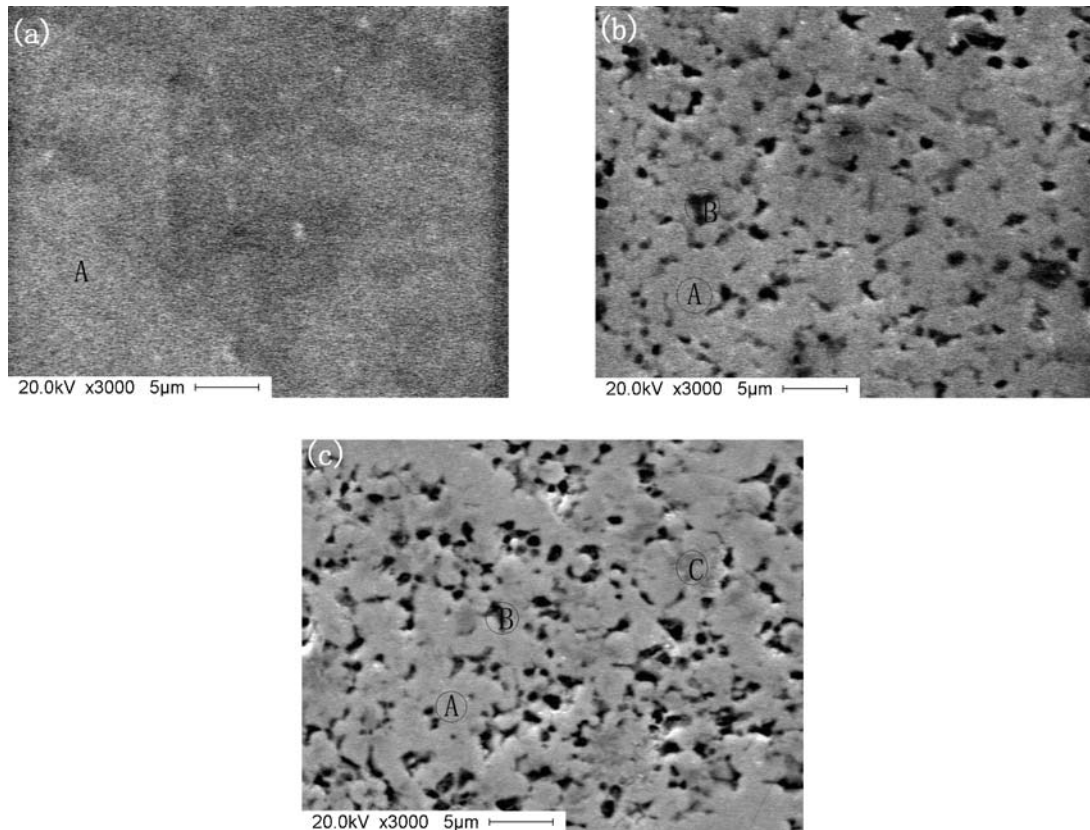


Figure 2 SEM images of as-cast  $\text{Nd}_{60}\text{Fe}_{20}\text{Co}_{10}\text{Al}_{10-x}\text{B}_x$  alloys (a)  $x = 0$ , (b)  $x = 2$ , and (c)  $x = 5$ .

$x = 0, 2, 5$ ) alloys are shown in Fig. 3. Some characteristic features can be seen: (1) There is a wide exothermic reaction peak over the temperature range from 600 to 750 K for  $\text{Nd}_{60}\text{Fe}_{20}\text{Al}_{10}\text{Co}_{10}$ . After 2–5 at.%B was added, the wide exothermic peak disappeared. (2) An exothermal peak related to crystallization is clearly found in all the DSC curves, indicating that these samples are mainly composed of amorphous phase, which is in agreement with the results of XRD. (3) Neither a glass transition nor a supercooled liquid region before crystallization are observed for  $x = 0, 2$ , and 5 alloys. (4) The crystalline temperature  $T_x$  decreases with addition of 2 at.%B. Further increase of B content has no significant effect on the  $T_x$ . (5) The endothermic peaks associated with melting can be seen for the  $\text{Nd}_{60}\text{Fe}_{20}\text{Al}_{10-x}\text{Co}_{10}\text{B}_x$  ( $x = 0, 2, 5$ )

as-cast alloys. The melting process changes from two steps to a single step when B content is increased to 5 at.%.

It is interesting to note that the wide exothermic reaction peak ranging from 600 to 750 K for  $\text{Nd}_{60}\text{Fe}_{20}\text{Al}_{10}\text{Co}_{10}$  disappeared after B was added. For the  $\text{Nd}_{60}\text{Fe}_{20}\text{Al}_{10}\text{Co}_{10}$  bulk amorphous alloy, Wei *et al.* [4] have pointed that the amorphous phase is a highly inhomogeneous system on the nanometer scale. The appearance of a wide temperature range corresponds to multi-stage crystallization as a result of composition inhomogeneity. According to the results of XRD and SEM, B additions lead to crystallization of regions of the amorphous phase.

Fig. 4 shows hysteresis loops as a function of B content for the Nd-Fe-Al-Co-B alloys. All of the

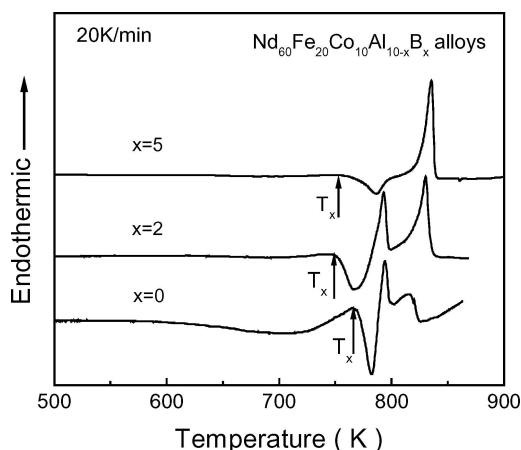


Figure 3 DSC curves of as-cast  $\text{Nd}_{60}\text{Fe}_{20}\text{Co}_{10}\text{Al}_{10-x}\text{B}_x$  ( $x = 0, 2, 5$ ) alloys.

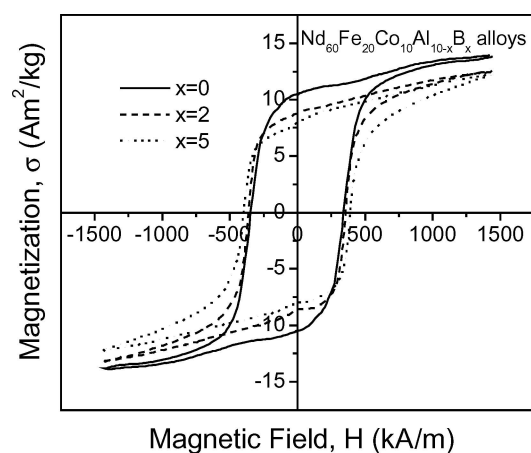


Figure 4 Hysteresis loops of as-cast  $\text{Nd}_{60}\text{Fe}_{20}\text{Co}_{10}\text{Al}_{10-x}\text{B}_x$  ( $x = 0, 2, 5$ ) alloys.

TABLE II Comparison of hard magnetic properties for  $\text{Nd}_{60}\text{Fe}_{20}\text{Al}_{10-x}\text{Co}_{10}\text{B}_x$  ( $x = 0, 2, 5$ ) alloys

| $\text{Nd}_{60}\text{Fe}_{20}\text{Al}_{10-x}\text{Co}_{10}\text{B}_x$ | $iH_c$ (k A/m) | $\sigma_s$ ( $\text{Am}^2/\text{kg}$ ) | $\sigma_r$ ( $\text{Am}^2/\text{kg}$ ) |
|--|----------------|--|--|
| $x = 0$  | 346            | 13.80                                  | 10.45                                  |
| $x = 2$  | 363            | 13.10                                  | 8.85                                   |
| $x = 5$  | 389            | 12.12                                  | 8.07                                   |

alloys show hard magnetic behavior at room temperature regardless of the coexistence of amorphous and crystalline phases for as-cast  $\text{Nd}_{60}\text{Fe}_{20}\text{Al}_{10-x}\text{Co}_{10}\text{B}_x$  alloys. It is suggested that the hard magnetic properties are not dependent on the amount of amorphous phase in the alloy. Substituting B for Al significantly increased the intrinsic coercivity ( $iH_c$ ) from 346 kA/m for  $x = 0$  to 389 kA/m for 5 at.% B addition, while the saturation magnetization ( $\sigma_s$ ) and remanence ( $\sigma_r$ ) decrease monotonously from 13.80 to 12.12  $\text{Am}^2/\text{kg}$  and 10.45 to 8.07  $\text{Am}^2/\text{kg}$ , respectively (also see Table II).

In  $\text{Nd}_{60}\text{Fe}_{20}\text{Al}_{10-x}\text{Co}_{10}\text{B}_x$  ( $x = 2, 5$ ) alloys, an amorphous phase coexists with a relatively high volume fraction of crystalline phases such as Nd and  $\text{NdFe}_4\text{B}_4$ , which are paramagnetic at room temperature [8]. Therefore, the high coercivity of  $\text{Nd}_{60}\text{Fe}_{20}\text{Al}_{10-x}\text{Co}_{10}\text{B}_x$  alloys is mainly attributed to the amorphous phase. According to the cluster model of the Nd-Fe magnetic system [9], the high coercivity of the cast  $\text{Nd}_{60}\text{Fe}_{20}\text{Al}_{10}\text{Co}_{10}$  bulk amorphous alloy originates from the magnetic exchange coupling interaction among the magnetic clusters with large random anisotropy. The coercivity of this magnetic system is determined by the number and the size of the magnetic clusters [10, 11]. Thus, it may be expected that an increase in the coercivity is due to an increase in the number and size of the ferromagnetic clusters in the amorphous phase as B substitutes for Al. The structure of the ordered clusters in the  $\text{Nd}_{60}\text{Fe}_{20}\text{Al}_{10-x}\text{Co}_{10}\text{B}_x$  ( $x=2, 5$ ) alloys is the subject of future investigations. The precipitation of the Fe-rich phase ( $\approx\text{Nd}_{44}\text{Fe}_{44}\text{Al}_3\text{Co}_9$ ) from the amorphous matrix of  $\text{Nd}_{60}\text{Fe}_{20}\text{Al}_5\text{Co}_{10}\text{B}_5$  alloy can

decrease the concentration of Fe content in the amorphous phase, which results in an apparent decrease in  $\sigma_s$  and  $\sigma_r$ .

In conclusion, B substitution for Al for the as-cast  $\text{Nd}_{60}\text{Fe}_{20}\text{Al}_{10-x}\text{Co}_{10}\text{B}_x$  ( $x = 0, 2, 5$ ) alloys decreases the glass forming ability of the alloys. The as-cast  $\text{Nd}_{60}\text{Fe}_{20}\text{Al}_{10-x}\text{Co}_{10}\text{B}_x$  ( $x = 0, 2, 5$ ) alloys show hard magnetic behavior. The addition of B increases the intrinsic coercivity significantly while the saturation magnetization and remanence decrease monotonously at room temperature. The addition of B can lead to precipitation of an Fe-rich phase from the as-cast alloy, which results in an apparent decrease in  $\sigma_s$  and  $\sigma_r$ .

### Acknowledgments

The authors are grateful to the financial support of the National Natural Science foundation of China (Grant No. 50001007, 500371051).

### References

1. A. INOUE, T. ZHANG, A. TAKEUCHI and W. ZHANG, *Mater. Trans. JIM* **37** (1996) 636.
2. *Idem.*, *ibid.* **37** (1996) 99.
3. *Idem.*, *ibid.* **37** (1996) 1731.
4. B. C. WEI, W. LÖSER, L. XIA, S. ROTH, M. X. PAN, W. H. WANG and J. ECKERT, *Acta Mater.* **50** (2002) 4357.
5. G. J. FAN, W. LÖSER, S. ROTH, J. ECKERT and L. SCHULTZ, *J. Mater. Res.* **15** (2000) 1556.
6. H. Z. KONG, Y. LI and J. DING, *J. Magn. Magn. Mater.* **217** (2000) 65.
7. N. CHAU, N. H. LUONG, C. X. HUU, N. X. PHUC and N. H. DAN, *ibid.* **242-245** (2002) 1314.
8. J. DING, L. SI, Y. LI and X. Z. WANG, *Appl. Phys. Lett.* **70**(12) (1999) 1763.
9. K. SIRATORI, K. NAGAYAMA, H. INO, N. SAITO and Y. NAKAGAWA, *J. Magn. Magn. Mater.* **83** (1990) 341.
10. B. C. WEI, W. H. WANG, M. X. PAN, B. S. HAN and Z. R. ZHANG, *Phys. Rev. B* **64** (2001) 012406.
11. S. SCHNEIDER, A. BRACCHI, K. SAMWER, M. SEIBT and P. THIYAGARAJAN, *Appl. Phys. Lett.* **80** (2002) 1749.

Received 4 June 2004

and accepted 25 March 2005